



ELSEVIER

Contents lists available at ScienceDirect

Opto-Electronics Review

journal homepage: <http://www.journals.elsevier.com/opto-electronics-review>

An evaluation of the range-gated-imaging technology under dense aerosol environments

J.W. Cho*, Y.S. Choi, K.M. Jeong

Nuclear Robot and Diagnosis Team, Korea Atomic Energy Research Institute, 111, Daedeok-daero 989 beon-gil, Yuseong-Gu, Daejeon, 305-353, Republic of Korea

ARTICLE INFO

Article history:

Received 9 April 2018

Received in revised form 21 August 2018

Accepted 23 August 2018

Available online 13 September 2018

Keywords:

Aerosol

Contrast

Fog

Fukushima Daiichi nuclear power plant

ICCD camera

Range-gated-imaging system

Severe accident

Visibility

ABSTRACT

Range-gated-imaging system, which can be used to eliminate backscatter in strong scattering environments, is based on two high speed technologies. It uses high power, ultra-short pulse laser as the light source. And it opens the optical gate of an ICCD camera with a micro-channel-plate image intensifier in a very short time while the laser pulses reflected by the object is coming back to the ICCD camera. Using this range-gated-imaging technology, the effect of scattered light can be reduced and a clear image is obtained.

In this paper, the test results of the range-gated-imaging system under dense aerosol environments, which simulates environments in the reactor containment building when the severe accident of the nuclear power plant occurred, are described. To evaluate the observation performance of the range-gated-imaging system under such dense fog environment, we made a test facility. Fog particles are sprayed into the test facility until fog concentration is reached to the postulated concentration level of the severe accident of the nuclear power plant. At such dense fog concentration conditions, we compared and evaluated the observation performances of the range-gated-imaging system and the CCD camera.

© 2018 Association of Polish Electrical Engineers (SEP). Published by Elsevier B.V. All rights reserved.

1. Introduction

When there is a severe accident at a nuclear power plant, such as a LOCA (loss-of-coolant accident) or reactor core meltdown (meltdown of nuclear fuel loaded in the reactor pressure vessel), defined as a design basis accident, the visibility inside the reactor containment building falls sharply due to the mass leaking of a reactor coolant (high temperature/high pressure steam over 250 °C). The fresh water (or sea water) being sprayed from the core spray system to cool the reactor core is vaporized into hot steam when it hits high-temperature (surface temperature of about 250 °C or higher) structures, such as the reactor pressure vessel protecting the reactor core. As the vaporized high-temperature steam is cooling, it generates aerosol, and the visibility inside the reactor containment building becomes bad due to this aerosol (fog). According to test data in cases of severe accidents, the diameters of aerosol particles are in the range of 0.1 μm – 5.0 μm (±2 μm on average), aerosol concentration at 300 s elapse after occurrence of the accident is approximately 500 mg/m³, and the maximum aerosol concentration inside containment vessels is 5 g/m³ [1–3]. Based on the above

mentioned test data, the observation environment inside the reactor containment building in the case of a severe accident of the nuclear power plant is greatly limited by scattering aerosol particles that have an average diameter of about 2.0 μm [4], and the visibility is calculated as 4.0 m – 0.4 m when aerosol concentration is 0.5 g/m³ – 5 g/m³ [5].

In April and October 2015, robots, loaded with LED lamps and colour CCD cameras, investigated the surroundings of the PCV (primary containment vessels) in Unit 1 and Unit 3 reactor buildings of the Fukushima Daiichi Nuclear Power Plant [6,7]. These inspection videos, taken by the robots, demonstrate that it is difficult to observe the surroundings in some areas due to high-temperature steam. At the end of January 2017, the surroundings of the pedestal (supporting structure for the reactor pressure vessel) inside the PCV of Fukushima Daiichi Nuclear Power Plant Unit 2 reactor building were investigated using a guide pipe equipped with LED lamps and pan/tilt camera [8]. In this investigation video, as in the inspection videos of the PCV surroundings in the Unit 1 and Unit 3 reactor buildings, it was similarly difficult to identify the surroundings in some areas due to high-temperature steam. This was because the cooling water, which was poured to prevent re-criticality of the high-temperature fuel debris that presumably reside at the bottom of both the reactor pressure vessel and the PCV and to manage the cold shutdown, which maintains the temperature of the molten

* Corresponding author.

E-mail addresses: jwcho@kaeri.re.kr (J.W. Cho), yschoi@kaeri.re.kr (Y.S. Choi), kmjeong@kaeri.re.kr (K.M. Jeong).

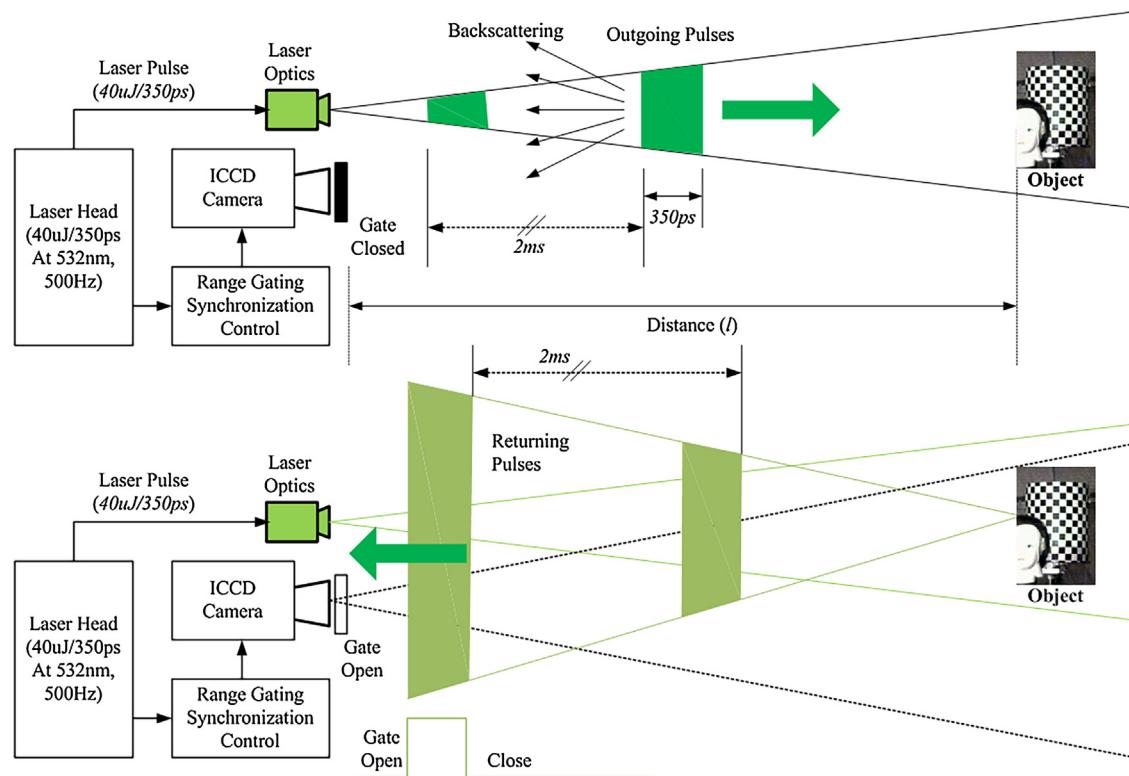


Fig. 1. Operation principle of the range-gated-imaging system.

reactor core below 100 °C, was vaporized into high-temperature steam by colliding with the hot fuel debris in meltdown state, and the steam obstructed the CCD camera's monitoring performance.

We reviewed the range-gated-imaging (RGI) technology as a way to overcome the limit of CCD camera observation performance in the dense aerosol environments generated inside a reactor containment building after a severe accident such as loss-of-coolant accident. In the RGI technology, an ultra-short pulse laser beam is irradiated to the object to be observed, and the images are obtained by opening the gate (shutter) of the ICCD (intensified CCD) camera at the instant the laser beam reflected from the object reaches the camera [9–11]. This allows us to obtain high-resolution observation images because it is influenced very little by scattering and diffuse reflectance caused by aerosol particles (fog or floating matter) in the space between the RGI observation system and the object [12,13].

In this paper, the observation characteristics of the RGI system were evaluated in a dense aerosol environment simulating a severe accident of the nuclear power plant, and the results are described. To simulate the dense aerosol environment due to the generation of aerosols in a severe accident, a test facility with width of 2.5 m, height of 2.5 m, and length of 15 m was set up. After fog particles were sprayed into the test facility, and the observation performances of colour CCD camera and the RGI system were compared and evaluated in the same fog concentration conditions.

2. Range gated imaging

As shown in Fig. 1, the laser module generates an ultra-short high-power laser pulse (40 μJ/350 ps) with a wavelength of 532 nm at a repetition rate of 500 Hz [14]. The ultra-short laser pulse of 350 ps reflects off the object and returns to the ICCD camera that has an electronic circuit for shutter (gate) control. The electronic circuit, which is controlling the shutter of the ICCD camera, opens the shutter synchronizing with the front (rising) part of the width of

the laser pulse that is reflected back from the object and closes the shutter synchronizing with the trailing (falling) part of the width of the laser pulse, and the ICCD camera obtains observation images of objects only within the range of the gate on/off pulse width time slot. For example, if the shutter on/off pulse width of the ICCD camera is 200 ps and the velocity of the light transmission is taken into account, the image acquisition range may be calculated as approximately 3 cm.

$$R_{im} = (c \times \Delta\tau_g) / 2 \quad (1)$$

In Eq. (1), R_{im} is the imaging range of the RGI system, c is the velocity of the light in the air, $\Delta\tau_g$ is the gate on/off pulse width of the ICCD camera. Images reflected back from an object located at a farther distance, which is a point after the shutter is closed, and images reflected back from an object located at a closer distance, which is before the shutter is opened, are not visible. As shown in Fig. 1, if the distance between the ICCD camera and the object is l , then the round-trip distance of the laser pulse is $2l$. The travel time of the laser pulse τ_l is expressed as Eq. (2).

$$\tau_l = 2l/c \quad (2)$$

To observe objects located at distance l , the shutter of the ICCD camera in the RGI system needs to be opened after τ_{on} as expressed in (3) and closed after τ_{off} as expressed in (4). The shutter open/close time span $\Delta\tau_g$ of the ICCD camera is variable depending on the volume of the object.

$$\tau_{on} = \tau_l \quad (3)$$

$$\tau_{off} = \tau_l + \Delta\tau_g \quad (4)$$

$$\Delta\tau_g = |\tau_{on} - \tau_{off}| \quad (5)$$

According to the literatures on the PCV surrounding inspections described in Refs. [6] and [7], the small robot system, which investigated the surroundings of the PCV in units 1 and 3 reactor buildings of the Fukushima Daiichi nuclear power plant, used 4 LED lamps

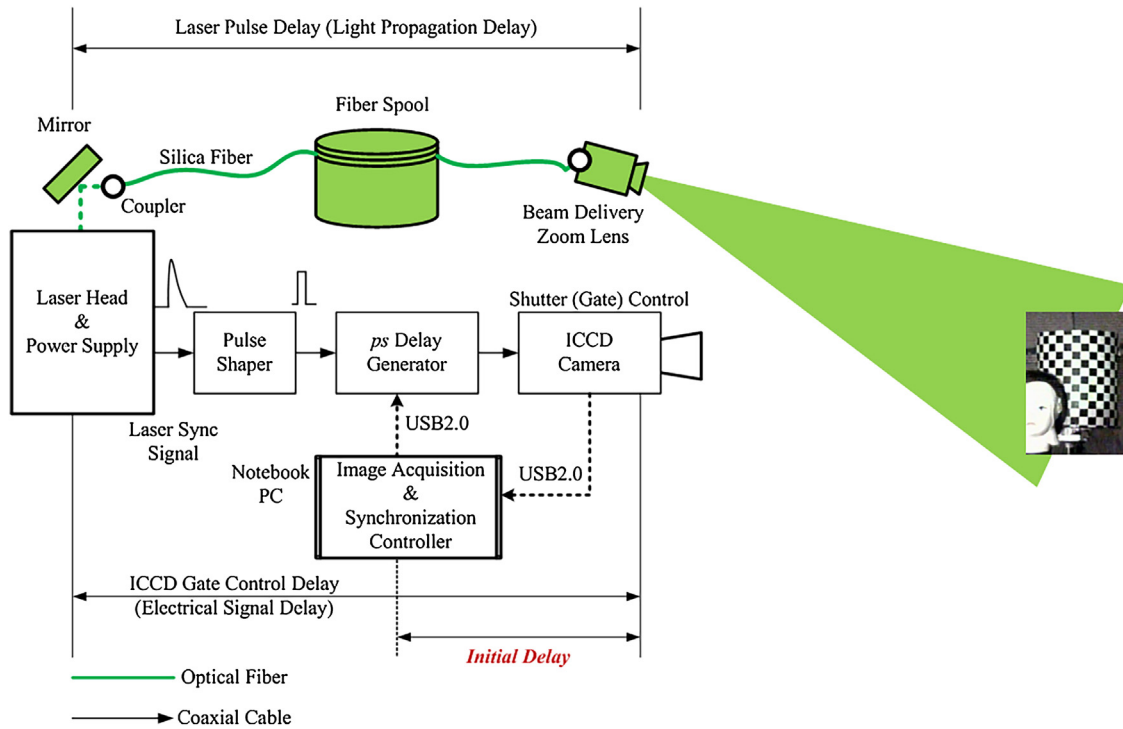


Fig. 2. Delay time of the range-gated-imaging system.

as the lighting source for the colour CCD camera, embedded in the inspection robot. Because the frame rate of the CCD camera is generally 30 Hz, the exposure time of the CCD sensor required to acquire one image is of about 33.3 ms. On the other hand, if the shutter open/close time span of the ICCD camera in the RGI system is equal to the laser pulse width of 350 ps and the sensitivity of the ICCD camera is equal to the CCD sensor, the quantities of light required for the ICCD camera should be approximately 95×10^6 times brighter than that required for the CCD sensor.

$$I_{ICCD} \varepsilon_{ICCD} = I_{CCD} \varepsilon_{CCD} \quad (6)$$

In Eq. (6), ε_{CCD} is an exposure time of the general CCD camera and ε_{ICCD} is an exposure time of the ICCD camera. A I_{ICCD} is the intensity of light required for the ICCD camera, I_{CCD} is the intensity of illumination for the CCD camera.

As such, because it requires an enormous quantity of light for a very short gate on/off time, the RGI system uses a high-power laser pulse as the light source. In this paper, the laser pulse output of the laser head is of $40 \mu\text{J}/350 \text{ ps}$. It is about 114.3 kW when converted into watts (J/s). This is about 10 000 times brighter than the intensity (12 W) of the 4 LED lamps for the CCD camera of the robot used to investigate the surroundings of the PCV in Units 1 and 3 of the Fukushima Daiichi nuclear power plant. From the calculation data, expressed in Eq. (6), the brightness of the laser pulse lighting alone does not satisfy the required quantity of light for the very short exposure time of the ICCD camera. So in this paper, an ICCD with a built-in MCP (micro channel plate, light amplification module) was used [15]. The minimum sensitivity, S_{ICCD} , of the ICCD camera is 10^{-7} foot candela (fc), and the dynamic range is ASA 50 to ASA 5×10^5 . When the minimum sensitivity of the ICCD camera is converted into watts, the minimum light intensity required per unit square meter is approximately as follows.

$$S_{ICCD} = 10^{-7} fc \cong 1.575 \times 10^{-9} \text{ W/m}^2 \quad (7)$$

$$1 fc = 10.76 \text{ lm/m}^2 \quad (8)$$

$$1 \text{ lm} = W/683 \quad (9)$$

The photosensitive area, A_{ICCD} , of the ICCD MCP (micro channel plate, light amplification module) is $14.4 \text{ mm} \times 11 \text{ mm}$ ($H \times V$). Therefore, the light intensity, I_{ICCD} , required for the MCP photosensitive surface of the ICCD camera should be greater than 0.25 pW as expressed in Eq. (10).

$$I_{ICCD} = A_{ICCD} S_{ICCD} \cong 0.25 \text{ pW} \quad (10)$$

Figure 2 shows the RGI layout used to calculate the system delay time of the RGI system. A propagation delay time of the ultra-short high-power laser pulse is about 300 ns when it passes through a mirror, a fiber optic spool (60 m length), and beam delivery & zoom lens. Because the refractive index of the silica-based optical fiber is about 1.5, the laser light propagates 1.5 times slower via the silica fiber than the air. In this paper, the propagation delay time of the laser pulse for the fiber optic spool was considered only, because the distance between the laser head and fiber coupler is very short compared to the 60 m fiber length. It means that a high power laser pulse, generated at the laser head module, is emitted in the air after about 300 ns.

As shown in Fig. 2, when a high power laser pulse is emitted from the laser head, a photo detector, equipped inside the laser head, converts optical signal (laser power) to an electrical sync signal indicating the emission of the laser pulse. A shape of the electrical sync signal, generated in the laser head module, is the analogue type. The analogue-typed electric sync signal follows just like the optical signal of the high power laser pulse. And the electrical sync signal of the laser head module is transmitted to the pulse shaper via coaxial cable. The pulse shaper converts an analogue sync signal to a digital (TTL) pulse signal. If the voltage of analogue sync signal is higher than the threshold voltage, it is high (5 V) TTL level. Else it is low (0 V) TTL level. The TTL sync signal of the pulse shaper is transmitted to the picosecond delay generator via coaxial cable. The picosecond delay generator outputs pulses with user-selectable delay and pulse duration, in respect to the falling edge of the pulse shaper TTL sync signal. The delay pulse of the picosecond delay generator is propagated to the ICCD camera via coaxial cable. It switches on/off the ICCD camera shutter (gate).

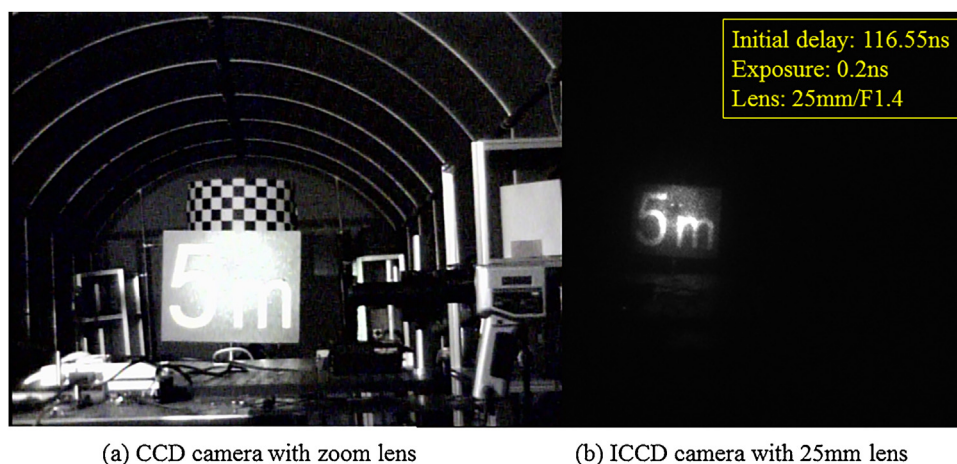


Fig. 3. 5 m target observation images of CCD and ICCD camera of the RGI system.

The system delay (electrical signal delay) time τ_g needed to switch on/off the gate of the ICCD camera is given in Eq. (11). The laser head module used in this paper does not control the output of the laser pulse by external trigger signal, so the internal sync (the sync signal that notifies the output of the laser pulse) of the laser head module was used. Therefore, in the system delay diagram shown in Fig. 2, the initial delay τ_{in} can be calculated using Eq. (12). In this paper, the initial delay was determined experimentally.

$$\tau_g = \tau_{co} + \tau_{in} \leq \tau_f \quad (11)$$

$$\tau_{in} = \tau_p + \tau_{dg} + \tau_{ICCD} \quad (12)$$

In Eq. (11), τ_f is the laser pulse propagation time passing through the optical fiber. And τ_{co} is the electrical signal transmission time of the coaxial cable, expressed as 3.3 ns/m. In (12), τ_p is the inherent delay time of the pulse shaping module. It is the system inherent time taken to convert the laser pulse shape of the laser head module into the TTL pulse. The inherent delay time of the picosecond delay generator is τ_{dg} , and τ_{ICCD} is the inherent delay time of the shutter control circuit of the ICCD camera.

The system delay time τ_g in Eq. (11) is the time it takes for the electrical trigger (sync) signal, generated when the ultra-short laser pulse is emitted from the laser head module, to pass through the pulse shaper, the picosecond delay generator and then to activate the gate (shutter) of the ICCD camera. Generally, the system delay time must be shorter than the propagation time of the laser pulse passing through the optical fiber.

$$\tau_g \cong \tau_f + \Delta\tau \quad (13)$$

As described in Eq. (13), if the system delay time is longer than the laser pulse propagation time by $\Delta\tau$, objects located within the round-trip propagation distance of the laser pulse corresponding to the time period of $\Delta\tau$ cannot be observed.

Figures 3 and 4 show comparative images of the CCD camera and RGI system. Fig. 3(a) shows images observed by the CCD camera equipped with a high-magnification zoom lens, and Fig. 3(b) shows images of objects observed by the RGI system at a distance of 5 m. In the RGI system, a 25 mm/F1.4 lens was attached to the ICCD camera. The initial delay time corresponding to a distance of 5 m was determined experimentally, and the exposure time (shutter open/close time span) of ICCD camera was set to 200 ps. Because the shutter open/close time span of the ICCD camera was set to 200 ps, the image shown in Fig. 3(b) is the observation image of the object within the range of about 5 m + 3 cm distance, calculated from (2).

Figure 4(a) shows images observed by the CCD camera equipped with a high-magnification zoom lens, and Fig. 4(b) shows images

of objects observed by the RGI system at a distance of 10 m. An 85 mm/F1.8 lens was used for the ICCD camera of the RGI system when observing objects at a distance of 10 m. The initial delay of 5 m target of the RGI system, shown in the upper right area of Fig. 3(b), is of 116.55 ns. And the initial delay time of 10 m target as shown in Fig. 4(b) is of 150.5 ns. The initial delay time difference between 10 m target and 5 m target is of 33.95 ns. Considering the round trip propagation distance of the laser light, the initial delay time difference of 33.95 ns is calculated about 5.1 m distance using Eq. (2).

From the initial delay time difference, shown in the upper right area of Figs. 3(b) and 4(b), we can know that the 10 m target image, observed by the RGI system, is 5 m distant from the 5 m target image, observed by the same RGI system, in reality.

3. Experiments and results

A test facility was built, as shown in Fig. 5, to simulate the dense aerosol environment in reactor containment buildings that may arise after a severe accident of the nuclear power plant, and to verify the observational characteristics of the RGI system. The test facility is 15 m in length (control room 2.5 m + fog room 12.5 m), 2.5 m in width, and 2.5 m in height. As shown in Fig. 5, the control room contains the RGI system and data acquisition system. In the middle of the control room there are two open circular windows of a diameter of 120 mm. A high-power laser pulse beam is irradiated through one open circular window, and the laser pulse returning after being reflected off the object is received by the ICCD camera lens through the adjacent open circular window. The fog machines are in the centre of the test facility, and fog particles of about 1 μ m–2 μ m in diameter are emitted through small holes in the pipe connected to the left side of the fog generator.

As shown in Fig. 5, the CCD camera with zoom lens was placed on the front side of the fog room to compare the observation performance with the RGI system under dense fog environments. The test pattern, chessboard plate shown in Fig. 4(a), was used for evaluating the observation performance of the CCD camera in the dense aerosol environments. The chessboard plate for the observation performance evaluation of the CCD camera, shown in Fig. 4(a), is about 3 m distant from the control room.

For the quantitative evaluation of the CCD camera monitoring performance under dense aerosol environments, the image contrasts of the black and white chess board pattern were calculated. After the fog particles emitted from the fog generator connection pipes filled the front area of the fog room, and they spread to the rear region of the fog room. Because the fog particles blocked the

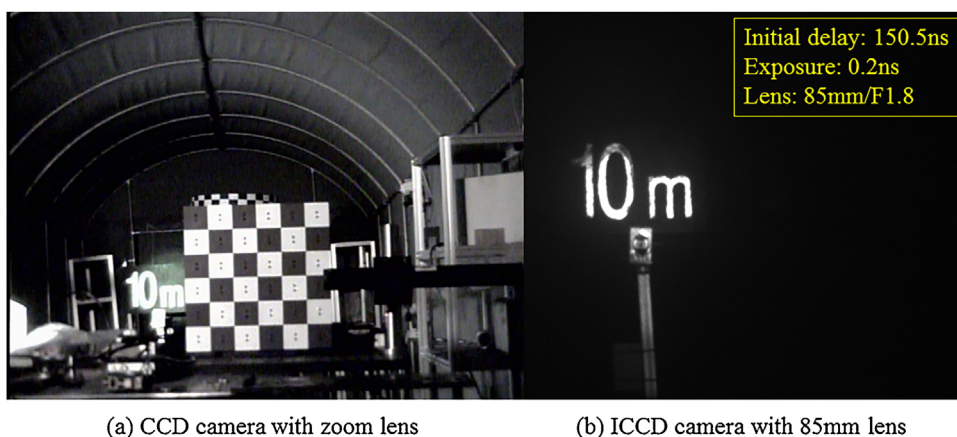


Fig. 4. 10 m target observation images of CCD and ICCD camera of the RGI system.

Experimental Setup (Top View)

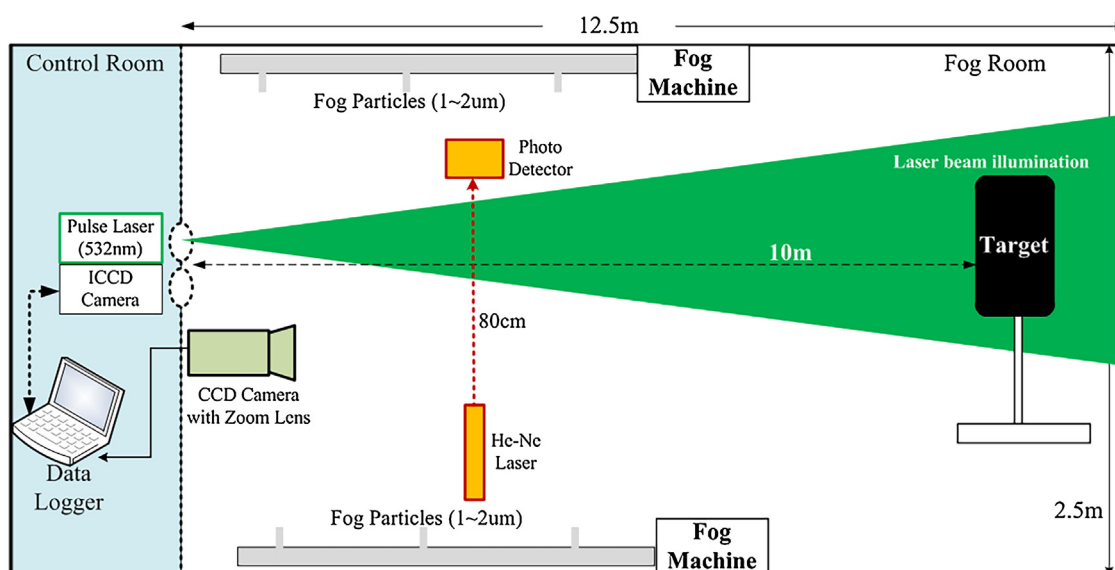


Fig. 5. A experimental setup for the RGI system evaluation under dense aerosol environments.

light, there was little light in the area where the target was located, which was about 10 m from the control room.

In this paper, a visibility was introduced as a criterion for comparing the observation performance of the RGI system and CCD cameras. To quantitatively calculate the visibility, the attenuation of the He-Ne laser light was measured in the dense aerosol environment. This is shown in the middle of the Fig. 5. Figure 6 depicts that the measurement scene of the laser beam attenuation of the He-Ne laser in the fog room under fog spray environments.

When fog particles were diffused onto the light path between the He-Ne laser source and the photo detector, the intensity of light measured by the photo detector decreased. The intensity of the He-Ne laser light before the fog spray is I_0 . The intensity of the He-Ne laser light is reduced due to the scattering after the fog spray. If we define the intensity of the He-Ne laser light at this time as I , then the visibility ν can be calculated as follows because we already know the distance L between the He-Ne laser source and the photo detector [16].

$$\nu = 2.995732/\varepsilon \quad (14)$$

$$\varepsilon = \ln(I_0/I)/L \quad (15)$$

In Eqs. (14) and (15), ε is the extinction coefficient and L is the distance between the He-Ne laser source and the photo detector. Fig. 7 shows the results of measuring the attenuation of the He-Ne laser power by the scattered fog particles, and Fig. 8 shows the visibility, calculated by Eqs. (14) and (15). In Fig. 7, the X axis represents the measurement time (sampling at 1 s interval), and the Y axis, displayed as a log scale, represents the power of the He-Ne laser measured by the photo detector. To simulate the dense aerosol environment, fog particles were sprayed for about 10 min. After then, the observation characteristics of the RGI system and CCD camera were compared in a steady state. In the transient state, as shown on the left side of Fig. 7, the intensities of the He-Ne laser measured by the photo detector were variable according to the fluctuation of fog particles, and as a consequence, the results of the visibility calculation also varied greatly.

Figure 9 shows two CCD camera observation images in the air before the fog spray. Fig. 9(a) shows a chessboard plate, 3 m distant from the control room, observed by the CCD camera with zoom lens located in the front area of the fog room. Fig. 9(a) represents the observation image of the CCD camera in air environments after the fog particles are sprayed right now in the fog room. Fig. 9(b) shows the chess board images observed by the CCD camera at about



Fig. 6. A laser beam attenuation measurement of the He-Ne laser in the fog room under fog spray environments.

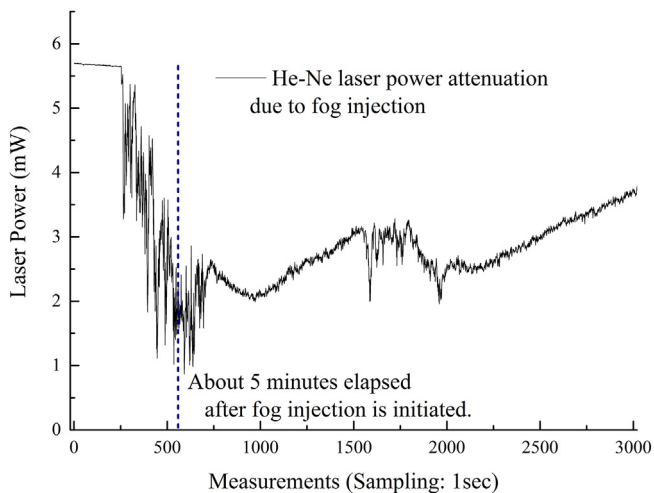


Fig. 7. An attenuation profile of the He-Ne laser power under fog spray environments.

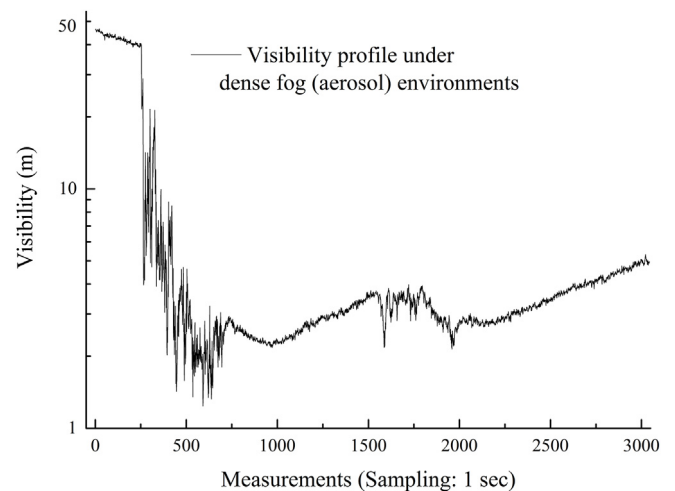


Fig. 8. Visibility distribution profiles in the fog room under fog spray environments.

23.5 min elapse after the fog spray started. In the case of the CCD camera observation image shown in Fig. 9(b), we can identify the chess board located at a distance of 3 m, but it is impossible to detect objects more than 3 m distance from the CCD camera.

Figure 10 show an observation images of a target (signboard) located at a distance of 10 m by the RGI system at the same observation time of the CCD camera. In Fig. 10(a), the MCP (micro channel plate) gain of the ICCD camera was set to minimum 600 V. The minimum MCP gain 600 V of the ICCD camera is more 100 times than the sensitivity of the general CCD camera. In air environments, because

the laser beam intensity reflected back from 10 m distant target surface is very strong, the observation image of the ICCD camera is saturated at the minimum image acquisition condition of the RGI system, as shown in Fig. 10(a). In dense aerosol environments, a 10 m distant target is dimly observed as shown in Fig. 10(b). The observation condition of the RGI system is represented at the upper right area of the Fig. 10(b). Because the laser beam intensity reflected back from a 10 m distant target surface is very weak due to the strong scattering of the dense fog particles in the fog room, we

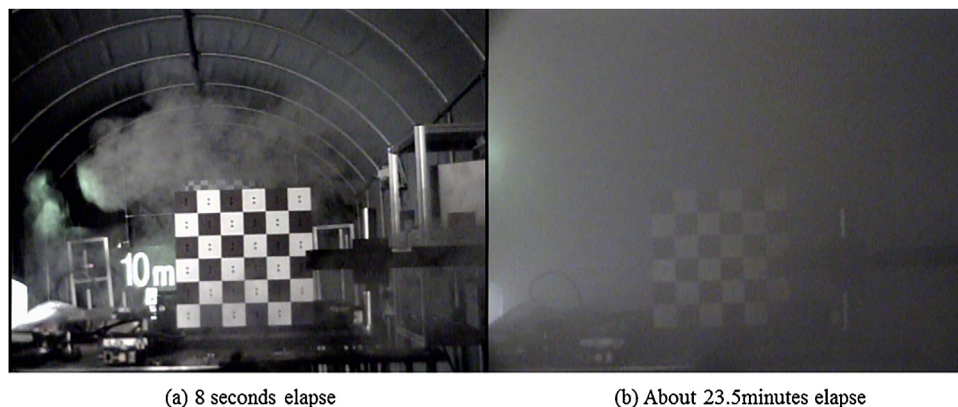


Fig. 9. A 3 m distant chessboard image observed by the CCD camera with zoom lens.

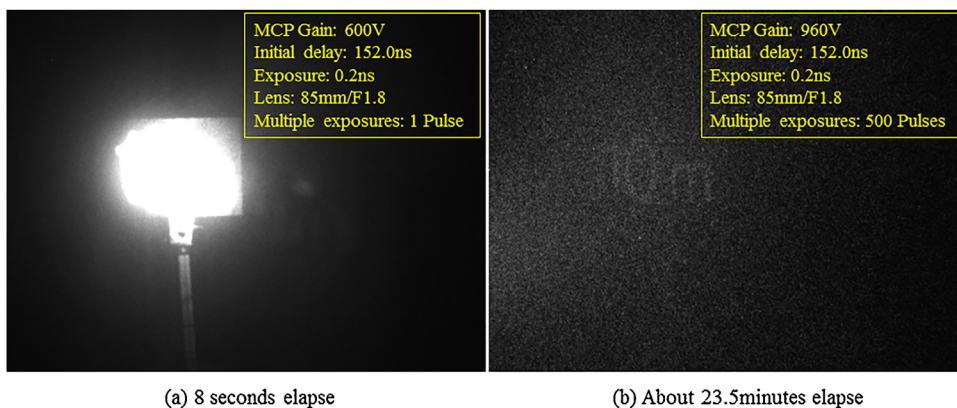


Fig. 10. A 10 m distant target image observed by the ICCD camera of the RGI system.

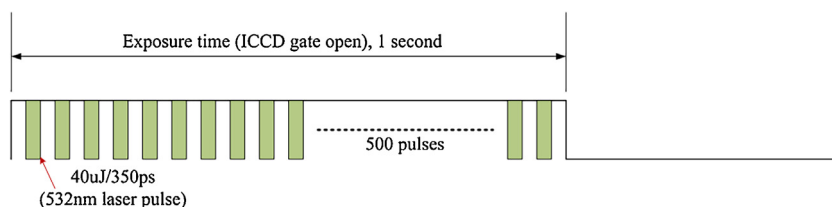


Fig. 11. A diagram of the multiple exposure technique.

used multiple exposures technique shown in Fig. 11. At this time, the visibility in the fog room was calculated as about 3.45 m.

As shown in Fig. 11, when the shutter of the ICCD camera is being opened during 1 s, 500 pulses of the laser beam reflected back from a 10 m distant target surface are accumulated in the ICCD sensor. Assumed that the laser intensity of the target surface is a little more intense than background, an accumulation of the multiple laser pulses reflected back from 10 m distant target surface can enhance observation performance of the ICCD camera.

When image contrasts were calculated using the contrast I_c in Eq. (16), the image contrast of Fig. 9(a) was of 0.62, and the image contrast observed at about 23.5 min elapse after the fog spray, shown in Fig. 9(b), was of 0.11. When the image contrast is lower than 0.07, we cannot identify chessboard pattern located at 3 m distant from the CCD camera. In Eq. (16), I_w is the brightness of the white area in the chess board pattern, and I_b is the brightness of the black area.

$$I_c = (I_w - I_b)/(I_w + I_b) \quad (16)$$

In case of the observation image of the RGI system as shown in Fig. 10(b), the MCP gain of the ICCD camera was set to maximum 960 V. In this case of the MCP gain 960 V, the sensitivity of the ICCD camera about 400 times higher than that of the MCP gain 600 V, shown in upper right area of the Fig. 10(a). In the dense aerosol environments of the fog room, a total sensitivity of the ICCD camera at the maximum observation condition of the RGI system was increased about 200 000 (400×500 pulses) times compared with the minimum observation condition after the fog spray is started just now, as shown Fig. 10(a). The intensities of the laser pulse power were severely attenuated due to the scattering caused by the fog particles, and, thus image processing technique was required in order to identify the features of the target (signboard). The image shown in Fig. 12 represents the processing image by the accumu-



Fig. 12. A result image of the accumulated summation method.

lated summation method using multiple images, expressed in Eqs. (17) and (18).

$$I_{ACC} = \sum_{i=1}^n I_i \quad (17)$$

$$\text{If } I_{x,y} > \text{threshold}, I_{x,y} = I_{x,y}, \text{ else } I_{x,y} = 0 \quad (18)$$

In Eqs. (19) and (20), I_i is the i_{th} image, $I_{x,y}$ is the gray level at 2D (x, y) image coordinates of the i_{th} image. And n is the number of the images used by the accumulated summation method.

Figure 12 shows the result image of the accumulated summation method, expressed in Eq. (17). In this study, the accumulation summation method used 5 images captured by the RGI system at the maximum observation condition, shown in Fig. 10(b). In Fig. 12, the left side of the target represents the laser beam scattering by the fog particles near the target located 10 m distant from the ICCD camera in the control room. The average visibility calculated in the dense

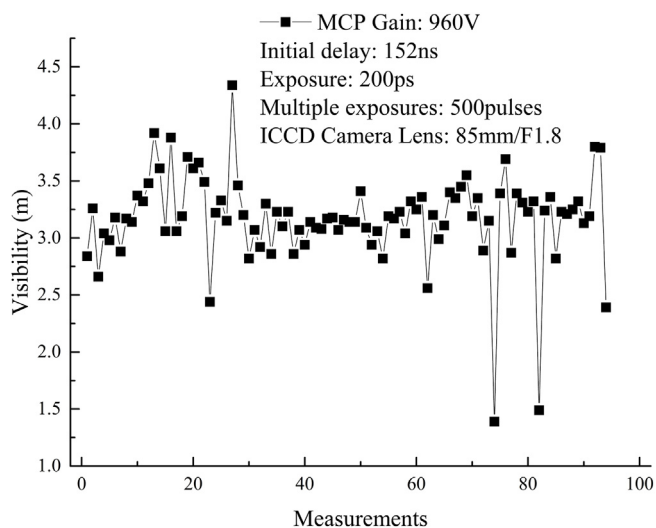


Fig. 13. Minimum visibilities profile of 10 m target identification by the RGI system.

fog environments for about 23.5 min after fog spray initiation was approximately of 3.45 m, and the visibility fluctuation ranged from a minimum of 2.85 m to a maximum of 4.29 m. Assumed that the average visibility in the fog room was of 3.45 m, the extinction coefficient calculated from Eq. (15) was approximately of 0.868. When the round-trip propagation distance of the laser light was taken into account, the brightness I_{3m} of the chess board target located at a distance of 3 m, detected by the CCD camera, was reduced to about $1/183$ of the brightness I_0 in the air before the fog spray. For the target located at a distance of 10 m, observed by the RGI system, the brightness I_{10m} of the target (signboard) decreased by 2.89×10^{-8} from the brightness before the fog spray.

$$I_{3m} = I_0 e^{-2\epsilon l} \approx 0.0055 I_0, \quad l = 3m, \quad \epsilon = 0.868 \quad (17)$$

$$I_{10m} = I_0 e^{-2\epsilon l} \approx 2.89 \times 10^{-8} I_0 \quad (18)$$

If the RGI system is to observe an object located at a distance of 10 m in these conditions with a visibility of about 3.45 m, it needs to have a sensitivity of about 52.8 dB (190 000 times) or more compared with the CCD camera, which is observing an object at a distance of 3 m.

Because the test facility was located outdoors, the visibility in the steady state did not drop below the visibility expected at the initial stage of a severe accident of the nuclear power plant (approximately of 4.0 m) when the experiment was conducted during the daytime, because it was affected by solar radiation. To exclude the effects of solar radiation, experiments were conducted mainly before sunrise or after sunset and on rainy or cloudy days at day time [17]. Figure 8 shows the visibility distribution measured at dawn. This indicates that the visibility was maintained within the range of 3 m in the steady state after the fog spray was ended.

Figure 13 show results of the experiments conducted after sunset, before sunrise, and during daytime.

In Fig. 13, the X-axis represents the number of measurements, and the Y-axis represents minimum visibility (m) for the RGI system to identify the features of a target (signboard) located at a distance of 10 m. The measurement conditions for these were MCP gain 960 V (maximum), initial delay of 152 ns (determined experimentally), exposure time (gate on/off) of 200 ps, and multiple exposures of 500 laser pulses/second. An 85 mm/F1.8 lens was attached to the ICCD camera. After conducting the experiments about 96 times, the average of the identifiable minimum visibilities of the target (signboard), located at 10 m distance from the RGI system in the control room, was found to be approximately of 3.17 m. The above-mentioned experimental results confirm that the RGI technology

exhibited an observation performance of three times or more than that of the CCD camera in a dense aerosol environment. In case of CCD camera, an object at a distance of 3 m can be observed at the visibility condition more than the average 3.17 m. But we cannot identify the objects more than 3 m distance from the CCD camera in the dense aerosol environments.

4. Conclusions

In this paper, we have attempted to verify the observational characteristics of the RGI system in the dense aerosol environment following a severe accident of the nuclear power plant. For this purpose, an outdoor test facility of width of 2.5 m, height of 2.5 m, and length of 15 m was set up to simulate the dense aerosol environment, which the visibility is less than 4 m, caused by the massive aerosol generated at the initial stage of a severe accident of the nuclear power plant. After the fog particles were sprayed into the test facility, the observation performances of CCD camera and the ICCD camera of the RGI system were compared and evaluated at the same visibility conditions.

Because the test facility is located outdoor, to match the visibility conditions of the initial stage of the severe accident of the nuclear power plant, experiments were performed mainly before sunrise or after sunset and in daytimes on rainy or cloudy days to avoid solar radiation. As a quantitative measure, we introduced the visibility which is calculated by the attenuation measurement of the He-Ne laser power under the dense aerosol environments of the test facility. The observation performance of CCD camera and observational characteristics of the RGI system were compared in steady state after fog particles were sprayed into the test facility for more than 10 min.

In case of the CCD camera, the image contrast of a target (chess board) located at a 3 m distance from the CCD camera was about 0.11 at the 3.45 m visibility condition. We can identify the target. But in the dense fog environments where visibility was less than 2.4 m, the image contrast was below 0.03, we cannot identify a 3 m target from the CCD camera observation image. In case of the ICCD camera of the RGI system, the target (signboard) located at a distance of 10 m was identifiable in an environment where visibility (average) was greater than 3.17 m. Therefore, the RGI system can be a useful observation method in the dense aerosol environment inside the reactor containment building, which is environment where visibility is limited to less than 4 m due to the massive generation of aerosol at the initial stage of a severe accident of the nuclear power plant.

Acknowledgement

This work was supported by the National Research Foundation of Korea (NRF) grant funded by the korean government (MSIP) (NRF-2012M2A8A1029350).

References

- [1] A.L. Wright, J.H. Wilson, P.C. Arwood, Pretest aerosol code comparisons for LWR aerosol containment tests LA1 and LA2, 2nd Int. Aerosol Conf (1986) 22–26.
- [2] D.A. Powers, J.L. Sprung, A Simplified Model for Aerosol Scrubbing by a Water Pool Overlying Core Debris Interacting With Concrete, Sandia National Lab., Albuquerque, NM, USA, 1993, NUREG/CR-5901, Nov.
- [3] H.J. Allelein, et al., State-of-the-art Report on Nuclear Aerosols, NEA/CSNI/R(2009)5, 2009.
- [4] S. Nomoto, Variations of visibility (Japanese), Denki 23 (1976) 234–257.
- [5] Visibility and air pollution, Air Pollution Handbook, McGraw-Hill, 1956, Chap. 6.
- [6] TEPCO, Tokyo, Japan, Apr. 30 Investigation Results at the Pedestal Grating Upper Area in the Unit 1 Reactor of the Fukushima Daiichi Nuclear Power Station (Japanese), Presented at the TEPCO Meeting (2015).

- [7] TEPCO, Tokyo, Japan, Oct. 20 Investigation Results Inside the PCV (Primary Containment Vessel) in the Unit 3 Reactor of the Fukushima Daiichi Nuclear Power Station (Japanese), Presented at the TEPCO Meeting (2015).
- [8] TEPCO, Tokyo, Japan, Jan. 26 Investigation Results Inside the PCV (Primary Containment Vessel) in the Unit 2 Reactor of the Fukushima Daiichi Nuclear Power Station (Japanese), Presented at the TEPCO Meeting (2017).
- [9] E. Sato, J. Akizono, H. Takahashi, Design and Manufacture of a Test Apparatus of Underwater Laser Viewing System (Japanese), Technical Note, The port and harbour research institute, Ministry of Transport, Japan, 1996, March.
- [10] K. Ochiai, K. Nishimura, T. Yamada, T. Baba, Development of the laser radar surveillance system technology at long-distances with high-resolution under inclement weather (Japanese), MHI Tech. Rev. 42 (2005) 212–215.
- [11] S. Donati, A. Sona, Evaluation of visibility improvements in fog by the range gating technique, Opto-Electron. 1 (1969) 89–101.
- [12] E. Belin, Display of an analytical model for backscattered luminance and a full-field range gated imaging system for vision in fog, Proc. SPIE 7088 (2008) 708800–1.
- [13] Y. Grauer, Active gated imaging in driver assistance system, Adv. Opt. Technol. 3 (2014) 151–160.
- [14] Diode Pumped Solid State Power Chip NanoLasers User's Manual, Teem Photonics Inc.
- [15] Operating Manual for intensified CCD (ICCD) digital video camera system (4 Picos-DIG), Stanford Computer Optics Inc., [Online] Available: <http://www.stanfordcomputeroptics.com/>.
- [16] M.J. Pilat, D.E. Ensor, Comparison between the light extinction aerosol mass concentration relationship of atmospheric and air pollutant emission aerosols, Atmos. Environ. Pergamon Press 5 (1971) 209–215.
- [17] Climate Information Data, Korea Meteorological Administration, [Online] Available: <http://www.kma.or.kr/>.

Jai Wan Cho was born in Goryung, Korea in 1960. He received the B.E. and M.E. degrees in electronic engineering from Kyung Pook National University, Daegu, Korea, in 1982 and 1984 respectively. Since 1987, he has been with the Nuclear Robot and Diagnosis Team, Korea Atomic Energy Research Institute, where he is now a principal researcher. His research interests are in robot visions for nuclear emergency response robot system, nuclear integrity monitoring system, VLC (visible light communication), and radiation-hardened instrumentation & control systems for the nuclear power plant.

Young Soo Choi was born in Daegu, Korea in 1966. He received the B.E. and M.E. degrees in electronic engineering from Kyung Pook National University, Daegu, Korea, in 1991 and 1993 respectively. He received Ph. D. degree in electronic engineering from Chung Book National University, Cheongju, Korea in 2010. Since 1995, he has been with the Nuclear Robot and Diagnosis Team, Korea Atomic Energy Research Institute, where he is now a principal researcher. His research interests are in robot visions for nuclear emergency response robot system, underwater robot system for the inside inspection of the hot leg & cold leg pipe in the RCPB (reactor coolant pressure boundary) area, and radiation-hardened vision systems for the nuclear power plant.

Kyung Min Jeong was born in Jeonju, Korea in 1966. He received the B.S. degree in mechanical design and production engineering from Seoul National University in 1988, and the M.S. degree in Production Engineering from the Korea Advanced Institute of Science and Technology (KAIST) in 1990 and the Ph. D. degree in Precision Engineering and Mechatronics from the KAIST in 1995. Since 1999, he has been with the Nuclear Robot and Diagnosis Team, Korea Atomic Energy Research Institute, where he is now a principal researcher. His research interests are in the walking robot for nuclear emergency preparedness, robust control, artificial intelligence, and vision and navigation systems for the nuclear power plant.